Journal Name

ARTICLE TYPE

Cite this: DOI: 10.1039/xxxxxxxxxx

Visualising the problems with balancing lithium-sulfur batteries by "mapping" internal resistance

Matthew J. Lacey,[a] Kristina Edström,[a] and Daniel Brandell[a]

Post-print accepted by Chem. Commun. Now published at doi: 10.1039/C5CC07167D

Received Date
Accepted Date

DOI: 10.1039/xxxxxxxxxx

www.rsc.org/journalname

Frequent and continuous determination of battery internal resistance by a simple current-interrupt method enables the visualisation of cell behaviour through the creation of resistance "maps", showing changes in resistance as a function of both capacity and cycle number. This new approach is applied here for the investigation of cell failure in the lithium-sulfur system with Li electrode excesses optimised towards practically relevant specifications.

The lithium-sulfur (Li-S) battery is currently one of the most intensely-studied "post-Li-ion" battery systems by virtue of its very high theoretical and practically achievable ($>$ 300 Wh kg^{-1} on the cell level) energy densities and the low cost of the active positive electrode material. However, relatively severe self-discharge and poor cycle life, which derive largely from the parasitic reactions of the soluble intermediates of the cell reaction - polysulfides - remain considerable challenges[1,2].

Much of the recent research in this regard has been directed towards optimisation of the positive electrode, for example through polysulfide encapsulation strategies or alternative host materials such as metal oxides. New electrolyte systems with extremely low solubilities for polysulfides have also been demonstrated. The negative electrode, however, has received relatively little attention. While the intrinsic inefficiency and dendritic morphology of lithium metal plating is well-documented[3–5], and the improved stability from alternative negative electrodes such as carbon and silicon has been reported[6,7], to the best of our knowledge there are no detailed studies in the literature so far on Li metal negative electrodes thin enough – that is, even closely balanced in capacity relative to the positive electrode – to meet the requirements of commercially viable cells. The negative electrode may have to be reduced to the order of 50 – 100%, according to at least one recent analysis[8]. There are compelling reasons to continue to focus on Li metal, however: it has the highest energy density of all the candidate negative electrode materials, and is likely to present fewer challenges for large-scale cell production compared to the alternative "Li-ion-sulfur" approach, which requires the use of either lithiated carbon or silicon, or lithium sulfide, as the lithium source - all of which are highly air-sensitive.

In this paper, we present a novel method for visualising and quantifying the changes in cell resistance to demonstrate the limitation on cycle life caused by a low excess of the Li metal electrode in the Li-S system.

Internal resistance is an important indicator of state-of-health and stability in batteries. There are a range of methods by which internal resistance can be estimated or determined, with electrochemical impedance spectroscopy (EIS) being the most commonly used in academic studies, especially in the Li-S field[9,10]. Other techniques include measuring the AC impedance at a single frequency (usually 1 kHz), pulsed galvanostatic methods[11] or current-interruption[12].

EIS is a powerful technique enabling the probing of the time dependence of different processes contributing to the total resistance, but one which requires specialist equipment and can very often be difficult to interpret correctly. This is especially true for the Li-S system, where the complexity in analysing data from EIS measurements is compounded by the complexity of the cell reaction itself. It has already been demonstrated in previous reports, for example, that the cell impedance changes significantly as a function of the state-of-charge[9,11,13,14]. It can also be a complex task to incorporate the measurements into extended battery testing procedures (e.g., galvanostatic cycling), as well as a time-consuming task to analyse large numbers of measurements correctly, especially if equivalent circuit fitting is used.

As such, while EIS is frequently used for comparisons of different materials, its use is usually relatively limited, for example to "before/after"-type comparisons or measurements on a relatively small number of cycles. For this reason it can for comparative

[a] *Department of Chemistry - Ångström Laboratory, Lägerhyddsvägen 1, SE-75121 Uppsala, Sweden. E-mail: matthew.lacey@kemi.uu.se*

† Electronic Supplementary Information (ESI) available: full experimental information, example voltage profiles and example R script for automated data analysis. See DOI: 10.1039/b000000x/

purposes be desirable to employ a simpler technique if it can be easily analysed (and visualised), and flexibly implemented into other testing procedures. In this work, we present such a technique, based on a current-interrupt method, with visualisation through "mapping" of the data as a function of both capacity and cycle number. This approach takes advantage of the programmability of modern battery cycling instruments and the possibilities for automated data analysis with freely available software packages to realise a powerful method to visually and quantitatively assess, in unprecedented detail, the electrochemical stability of batteries over extended usage.

The cells presented in this work comprise positive electrodes optimised towards high energy, prepared only from commercially available materials, and an optimised volume of the electrolyte. The positive electrodes were prepared using porous carbon black as the conductive host material and a water-based functional binder derived from our earlier work[15], and deliver a capacity of ~2 mAh cm^{-2} with a relatively high sulfur content (65% w/w total in the electrode). The electrolyte volume was minimised to the smallest possible volume (6 μL mg$_S^{-1}$) at which stable cycling was still possible. Lithium electrodes of 125 μm and 30 μm thickness were tested, representing theoretical capacities of 25.8 and 6.2 mAh cm^{-2} or >1000% and ~200% excesses of Li respectively. It is difficult to compare these values with the existing literature, since the electrolyte/sulfur ratio and the thickness of the negative electrode are, in most cases, not reported. Nonetheless, lithium foils of at least of 100 μm and possibly far thicker are standard choices in the laboratory, and most previous studies report sulfur electrodes with lower sulfur loadings and far greater electrolyte excesses than we report here[16]. Consideration of the electrolyte volume and anode excess are of particular importance, since the former is currently the most significant barrier to high practical energy density, and both are likely the main contributors to short cycle life. Full experimental details are given in the Supporting Information.

The performance of these cells using the two different negative electrode thicknesses is presented in Figure 1. Both cells were cycled until complete failure was apparent (e.g., from irregular voltage profiles, evidence of short-circuiting, etc.). From this figure the effect of the different negative electrodes is immediately apparent. With the thicker, high excess Li electrode, the cell shows a stable reversible capacity of 800 – 900 mAh g^{-1} for 120 cycles, and does not fade significantly before cell failure occurs. With the thinner, low excess Li electrode, however, the capacity follows the thick Li cell well over the first 10 cycles, then increases to a maximum at around 40 cycles, and then begins to fade rapidly, before failing altogether after 90 cycles. In terms of coulombic efficiency, both cells show the same coulombic efficiency of ~97% up to around 40 cycles, at which point the efficiency starts to decrease in both cells, but with a faster rate of decrease for the thin Li electrode. The coulombic efficiency drops to approximately 90% for both cells by the time cell failure occurs.

To follow the changes in internal resistance over cycling, current interruptions of 0.5 s were inserted into the C/10 cycling procedure every five minutes. Internal resistance was estimated from each individual interruption simply as $R = dE/dI$ over a

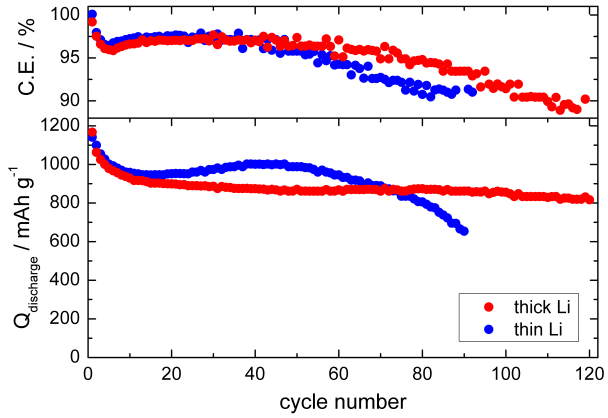

Fig. 1 Specific discharge capacity and coulombic efficiency vs cycle number for lithium-sulfur cells containing thick (125 μm) or thin (30 μm) Li foil negative electrodes cycled until failure.

fixed time. Example voltage profiles showing the frequency of the current interruptions and the determination of the voltage drop are given in the Supporting Information, Figure S1. The resistance determined from the current interruption technique over this timescale is approximately the sum of Ohmic electronic and ionic resistances in the electrodes and electrolytes and charge transfer (kinetic) resistances. A comparison of this technique with established impedance and current pulse techniques is given in the Supporting Information. The frequency at which measurements are taken gives 100 – 150 individual measurements of internal resistance in each cell per cycle; giving almost 16,000 measurements of resistance for the "thick Li" cell over the 120 cycles presented here. Analysis of these large datasets and the visualisation of the processed data is accomplished easily with a simple computer program written in the freely available programming language R. An example script for data analysis and plotting of the following figure is also given in the Supporting Information.

The results of this experiment, plotted as a heat map of capacity vs cycle number and colour-coded according to the measured resistance at each given point, are given in Figure 2. Note the direction of discharge and charge in reading along the capacity (y-) axis; in both cases the maximum capacity values (at the top of the plot frame) correspond to the fully discharged state, and minimum capacity values correspond to fully charged. In terms of the trends in cell resistance, there are a number of key observations that can be made from these maps alone:

- *Changing resistance during (dis)charge, and asymmetry of the charge/discharge reactions*: at a capacity of ~250 mAh g^{-1} there is a clear peak in the cell resistance, which is especially pronounced for the discharge cycle. This peak in resistance, which has also been described elsewhere[9], relates to the transition from the upper to the lower voltage plateau, where the concentration of polysulfides in the electrolyte reaches a maximum, or even supersaturates. The asymmetry of the discharge and charge reactions is also revealed. While a peak in resistance corresponding to the same transition is also visible in the charge process, it is broader and with a lower maximum. This is likely a result of the lower rate of

This journal is © The Royal Society of Chemistry [year]

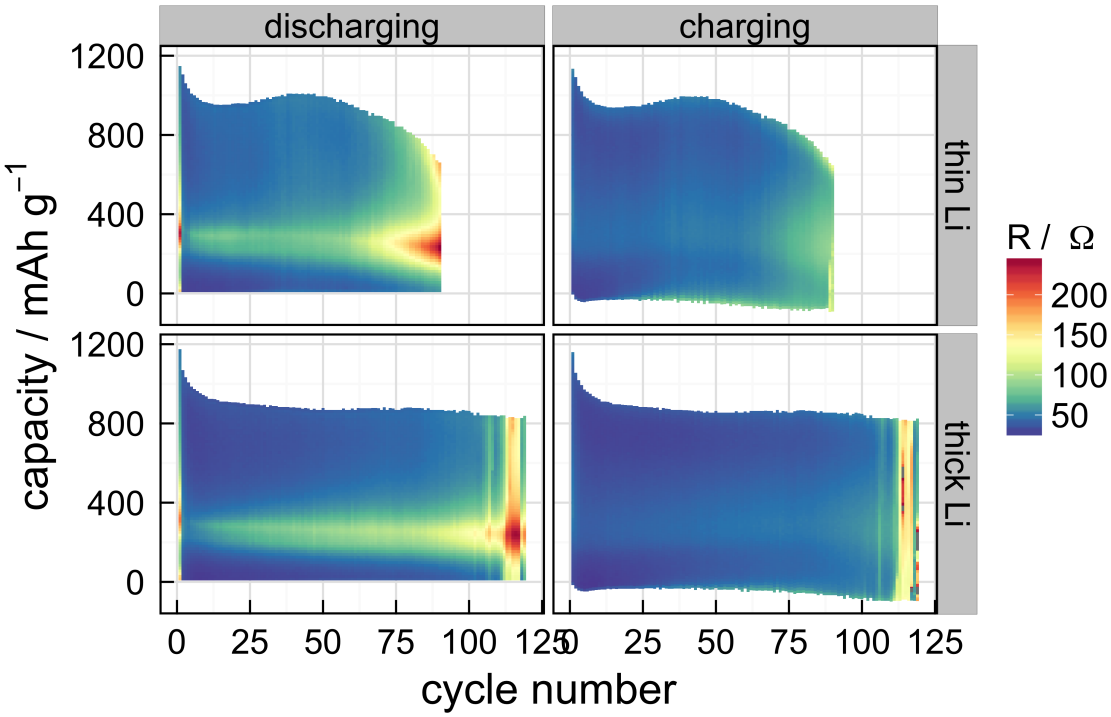

Fig. 2 Specific capacity vs cycle number plots for lithium-sulfur cells with different negative electrode thicknesses, coloured according to the calculated internal resistance at each given point.

change in polysulfide concentration on charging as opposed to discharging, consistent with what we and other groups have previously observed[17,18].

- *Rapidly increasing resistance before cell failure*: The internal resistances of the two cells are similar up until approximately cycle 60, at which point the gradual capacity fade of the cell with the thin Li electrode is accompanied with a rapid increase in resistance. The peak resistances for the thin Li cell reach ∼250 Ω, compared with values of ∼100 Ω over the first 50 or so cycles. The cell with the thick Li electrode, on the other hand, shows a similarly gradual increase in resistance over 100 cycles, with a more sudden rapid increase in resistance before cell failure. The maximum resistances for the cell reach similar values in both cells.

- *Indications of severe electrolyte decomposition*: For both cells, before any clear onset of cell failure, there are no indications of resistance increases at the charge or discharge limits. For the lower voltage plateau (i.e., $Q > \sim 300$ mAh g^{-1}), the resistance in fact remains relatively constant. This indicates that electrode passivation does not ordinarily determine the end points of charge or discharge. However, as the "thin Li" cell starts to show clear signs of failure (after approx. 70 cycles), the resistance begins to increase particularly close to the discharge end-point. That the resistance decreases again on the charge cycle indicates that the increase most likely relates to reversible behaviour of polysulfide species, perhaps rendered more poorly soluble by a changing electrolyte composition, as opposed to irreversible processes such as solvent decomposition. A possible interpretation, then, for the rapidly increasing resistance during cell failure is a combination of inactivated polysulfide species with a gradually decreasing conductivity of the electrolyte and/or passivation of one or both electrode surfaces by products of electrolyte decomposition[19]. Moreover, the increase in resistance prior to cell failure appears to be independent of capacity fade. The rapidly fading capacity for the "thin Li" case can be interpreted as a decreasing availability of Li due to the low excess; conversely, a large Li excess would then explain the relatively stable capacity of the "thick Li" cell. That the resistance increases similarly rapidly for both cells is further evidence that electrolyte consumption is responsible for cell failure, with said consumption occurring faster if the negative electrode excess is lower, with an increasingly unfavourable morphology of the lithium electrode the likely cause[19]. Simple strategies which target improved morphology of lithium, for example heavier alkali metal additives[20], may be particularly effective in this regard.

Clearer overall trends across extended cycling can be seen by simply taking the averages of the measured resistances within each cycle. The median resistances for each individual (dis)charge cycle calculated from the data in Fig. 2 are presented in Figure 3, from which further conclusions can be made about the changes in the resistances of the cells. Firstly, it can be more easily seen that the median cell resistance for both cells is approximately 90 Ω on the first discharge cycle, dropping to about half of this value on the first charge cycle. This resistance decrease is likely to be due to a combination of a relaxation of the positive

electrode with a minor contribution from the roughening of the negative electrode surface.

Secondly, it is clear from Fig. 3 that, following the first few cycles, the cell resistance increases approximately linearly for the "thick Li" cell over 100 cycles, before the resistance rapidly increases and the cell fails. For the "thin Li" case, the resistance follows the same trend, albeit with a slightly higher resistance, until around 60 cycles, after which the resistance increases rapidly. These observations reflect those made previously from Fig. 2. Fig. 3 also reveals that the median resistances are also slightly lower over the charge cycles than for the discharge cycles. This may reflect some asymmetry in the kinetics for the charge transfer reactions of the charge and discharge processes.

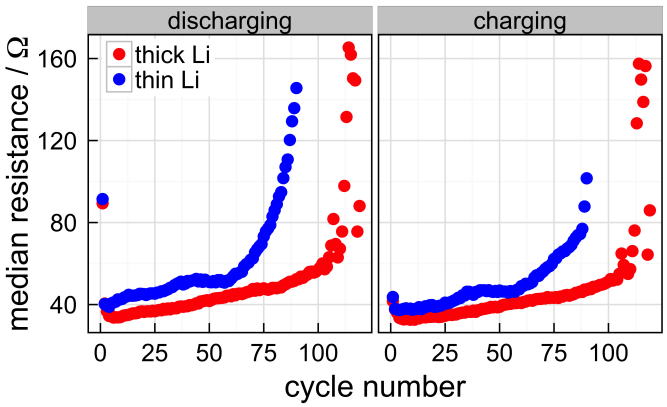

Fig. 3 Median internal resistance for each (dis)charge step vs cycle number, as calculated from the data given in Fig. 2.

In terms of the effect of reducing the negative electrode excess, the principal conclusion to be drawn from Fig 3 is very clear: the trends in the cell resistance for both cells are very similar, with a lower Li excess promoting earlier cell failure. There remain however several unanswered questions for future study. Firstly: while the capacity fading only in the "thin Li" case may be explained by a gradually decreasing availability of Li, the reason for the initially *increasing* capacity, which we have observed over numerous experiments with different positive electrodes, remains unclear. Furthermore, we note in the "thin Li" case that the resistance remains roughly constant or even decreases slightly between cycles 35 and 60. While a similar feature is not easily seen in the "thick Li" case presented here, we have observed similar temporary decreases in resistance in other cells studied with this technique, and the same effect was previously observed for Li-S cells using a sulfolane-based electrolyte[11]. However, the cause of this is also not yet clear. Further experiments are planned in the future to extend this method to three-electrode setups to clearly separate the contributions of the positive and negative electrodes.

In summary, we present here a novel approach to following and visualising the changes in internal resistance in batteries in high detail. This constitutes a simple and convenient technique for assessing the state-of-health and long-term stability of Li-S batteries, and is in principle extendable to any battery system. While the current-interrupt measurement requires assumptions which may result in deviations in the calculated resistance from the true value, for Li-S cells at least the trends are relatively insensitive to the timescale over which the voltage dropped is measured. Furthermore, the ease of which these measurements can be made with standard battery testing instruments and the convenience of completely automated data analysis with freely available software are considerable advantages: the time and expertise required for interpretation of EIS is not required, and the current-interrupt approach to estimating resistance lengthens the total measurement time only by $\sim 0.17\%$. This method is therefore a very convenient and powerful approach for simple evaluation of different cell configurations. This has been demonstrated here with a comparison of two Li-S cells with different negative electrode thicknesses, with the "thin" (30 μm thick) Li electrode in particular close to the low Li excess desired for commercially viable cells. The reduction of the Li excess clearly results in an earlier onset of cell failure, due to a rapidly increasing resistance, and severe capacity fade. The increasing resistance causing cell failure was attributed to electrolyte decomposition. It is important to note that the electrolyte volume used here was 6 μL g_S^{-1} – still in too high excess for commercially viable cells[16,21] – and that lower electrolyte volumes tested resulted in cell failure within just a few cycles. Cycle lifetime of $\sim$100 cycles is clearly too short for this system to be considered beyond niche applications, but is the inevitable consequence of optimising the amount of electrolyte and negative electrode to that required for high energy cells; it is therefore imperative that the issues resulting from reduced electrolyte and Li excess receive greater attention in future research.

Acknowledgements

The authors thank the Era Net Transport project "MaLiSu" and Vinnova in Sweden for financial support.

References

1 S. S. Zhang, *J. Power Sources*, 2013, **231**, 153–162.
2 A. Manthiram, S.-H. Chung and C. Zu, *Adv. Mater.*, 2015, **27**, 1980–2006.
3 R. Mogi, M. Inaba, S.-K. Jeong, Y. Iriyama, T. Abe and Z. Ogumi, *J. Electrochem. Soc.*, 2002, **149**, A1578.
4 D. Aurbach, *J. Electrochem. Soc.*, 1995, **142**, 2882.
5 R. Bhattacharyya, B. Key, H. Chen, A. S. Best, A. F. Hollenkamp and C. P. Grey, *Nat. Mater.*, 2010, **9**, 504–510.
6 J. Brückner, S. Thieme, F. Böttger-Hiller, I. Bauer, H. T. Grossmann, P. Strubel, H. Althues, S. Spange and S. Kaskel, *Adv. Funct. Mater.*, 2014, **24**, 1284–1289.
7 S. Thieme, J. Brückner, A. Meier, I. Bauer, K. Gruber, J. Kaspar, A. Helmer, H. Althues, M. Schmuck and S. Kaskel, *J. Mater. Chem. A*, 2015, **3**, 3808–3820.
8 D. Eroglu, K. R. Zavadil and K. G. Gallagher, *J. Electrochem. Soc.*, 2015, **162**, A982–A990.
9 N. A. Cañas, K. Hirose, B. Pascucci, N. Wagner, K. A. Friedrich and R. Hiesgen, *Electrochim. Acta*, 2013, **97**, 42–51.
10 Z. Deng, Z. Zhang, Y. Lai, J. Liu, J. Li and Y. Liu, *J. Electrochem. Soc.*, 2013, **160**, A553–A558.
11 V. Kolosnitsyn, E. Kuzmina and S. Mochalov, *J. Power Sources*, 2014, **252**, 28–34.
12 M. Kim and E. Hwang, *J. Power Sources*, 1997, **64**, 193–196.
13 C. Barchasz, J.-C. Leprêtre, F. Alloin and S. Patoux, *J. Power Sources*, 2012, **199**, 322–330.
14 C.-S. Kim, A. Guerfi, P. Hovington, J. Trottier, C. Gagnon, F. Barray, A. Vijh, M. Armand and K. Zaghib, *J. Power Sources*, 2013, **241**, 554–559.
15 M. J. Lacey, F. Jeschull, K. Edström and D. Brandell, *J. Power Sources*, 2014, **264**, 8–14.
16 M. Hagen, D. Hanselmann, K. Ahlbrecht, R. Maça, D. Gerber and J. Tübke, *Adv. Energy Mater.*, 2015, 1401986.
17 M. J. Lacey, K. Edström and D. Brandell, *Electrochem. Comm.*, 2014, **46**, 91–93.
18 M. Cuisinier, P.-E. Cabelguen, S. Evers, G. He, M. Kolbeck, A. Garsuch, T. Bolin, M. Balasubramanian and L. F. Nazar, *J. Phys. Chem. Letts.*, 2013, **4**, 3227–3232.
19 Y. V. Mikhaylik, I. Kovalev, R. Schock, K. Kumaresan, J. Xu and J. Affinito, ECS Trans., 2010, pp. 23–34.

This journal is © The Royal Society of Chemistry [year]

20 J. S. Kim, T. H. Hwang, B. G. Kim, J. Min and J. W. Choi, *Adv. Funct. Mater.*, 2014, 5359–5367.

21 M. Hagen, P. Fanz and J. Tübke, *J. Power Sources*, 2014, **264**, 30–34.